Research paper/

Sulfur hexafluoride and potassium bromide as groundwater tracers for managed aquifer recharge

Sarah Paschal Gerenday: Department of Earth Science, University of California Santa Barbara, Santa Barbara, CA, USA

Jordan F. Clark: Department of Earth Science, University of California Santa Barbara, Santa Barbara, CA, USA

Jeffrey Hansen: HDR Engineering, Inc., Olympia, WA, USA

Ida Fischer*: HDR Engineering, Inc., Seattle, WA, USA

John Koreny†: HDR Engineering, Inc., Seattle, WA, USA

Conflict of interest: None.

Key words: groundwater, infiltration, managed aquifer recharge, tracers, sulfur hexafluoride, bromide, trapped air, reclaimed water

Article impact statement: Understanding differences in tracer behaviors can inform permitting for managed aquifer recharge.

* Now at Aspect Consulting, Seattle, WA, USA
† deceased January 2019

Abstract

Sulfur hexafluoride (SF_6) is an established tracer for use in managed aquifer recharge projects. SF_6 exsolves from groundwater when it encounters trapped air according to Henry's Law. This results in its retardation relative to groundwater flow, which can help determine porous media saturation and flow dynamics. SF_6 and the conservative, non-partitioning tracer, bromide (Br^- added as KBr), were introduced to recharge water infiltrated into stacked glacial aquifers in Thurston County, Washington, providing the opportunity to observe SF_6 partitioning. Br^-, which is assumed to travel at the same velocity as the groundwater, precedes SF_6 at most monitoring wells. Average groundwater velocity in the unconfined aquifer in the study area ranges from 3.9 – 40 m/d, except in the southwestern corner where it is slower. SF_6 in the shallow aquifer exhibits an average retardation factor of 2.5 ± 3.8, suggesting an air to water ratio on the order of 10^{-3} to 10^{-2} in the pore space. Notable differences in tracer arrival times at adjacent wells indicate very heterogeneous conductivity. One monitoring well exhibits double peaks in concentrations of both tracers with different degrees of retardation for the first and second peaks. This suggests multiple flowpaths to the well with variable saturation. The confining layer between the upper two aquifers appears to allow intermittent connection between aquifers but serves as an aquitard in most areas. This study demonstrates the utility of SF_6 partitioning for evaluating hydrologic conditions at prospective recharge sites.

Introduction

Increasing populations and climate insecurity are forcing many municipalities to reevaluate how they manage their water supplies. One available strategy is to use treated wastewater for managed aquifer recharge (MAR) and eventual reuse. MAR is the addition of

water into aquifers by infiltration or injection at engineered facilities to prevent their depletion. MAR can be an efficient way of storing water and can provide an opportunity for contaminants to be removed or degraded through interaction with matrix materials and microbes (Bouwer 2002; P. Dillon 2005).

An important step in MAR projects planning to recharge reclaimed wastewater is to conduct a tracer study to establish subsurface residence times, as this timing affects the degree to which residual chemicals and pathogens in the reclaimed water will be attenuated before the water is re-extracted or discharges to surface water. Tracer data also serve to establish hydraulic connections between recharge and extraction facilities. Furthermore, tracers can be used to evaluate subsurface flow, groundwater ages, and hydrologic properties of aquifers.

This paper evaluates the behaviors of two tracers added to MAR water: sulfur hexafluoride (SF_6), a relatively insoluble gas tracer, and bromide (Br^-), a common ionic tracer. These chemicals are easy to distinguish from their background concentrations, and SF_6 can be detected at concentrations ranging over several orders of magnitude (Wanninkhof et al. 1987). Both tracers are non-toxic at the concentrations used and are chemically non-reactive. As an insoluble gas, SF_6 exsolves in the presence of trapped air, retarding its transport, while behaving conservatively under saturated conditions (Fry et al. 1995; Vulava et al. 2002). Bromide, on the other hand, behaves conservatively regardless of porous media saturation as demonstrated by numerous studies in the unsaturated zone (e.g., Flury and Wai, 2003). The use of these two tracers allows comparison of the behaviors of ionic and gas tracers and the evaluation of gas partitioning, which will aid in selecting the appropriate tracers in subsequent environmental investigations.

Although there have been several studies of SF_6 partitioning in laboratory experiments (Balcke et al. 2007; Bullister et al. 2002; Vulava et al. 2002) and various field studies employing the gas as a tracer (Clark et al. 2004, 2005; McDermott et al. 2008; K.Dillon et al. 1999), there have been few studies that make use of SF_6 partitioning in the field. Typically, it is assumed that SF_6 is conservative in groundwater; however, it is known that small pockets of air are routinely trapped in otherwise saturated porous media with implications for biological processes and infiltration rates (Christiansen 1944; Heilweil et al. 2004). Therefore, some degree of SF_6 partitioning may occur, which can provide a useful tool for understanding air distribution in porous media. This study examines SF_6 transport and partitioning in a set of stacked glacial aquifers with localized heterogeneities, which provides the opportunity to observe tracer behaviors in a natural setting and to shed light on the site's hydrologic properties.

Study location

This study was conducted at the Hawks Prairie Reclaimed Water Ponds and Recharge Basins managed by the LOTT Clean Water Alliance in Thurston County, Washington (Fig. 1). At the site are eight one-acre infiltration basins, two of which were used in the study. The Hawks Prairie site is underlain by the Vashon formation, which consists of Quaternary glacial siliciclastic deposits (Fig. 2). In the Vashon advance outwash is a shallow, unconfined aquifer. Flow is restricted in some locations by occurrence of Vashon Till. The shallow aquifer is separated by a confining unit of pre-Vashon sand and finer sediment, which is sometimes referred to as the Kitsap formation, from a gravel layer forming the sea level aquifer. The sea level aquifer is underlain by Tertiary mixed glacial and non-glacial deposits in which a deep aquifer occurs. Groundwater flow through the study area determined from monitoring well head measurements in the shallow aquifer is predominately to the south and southwest, and flow in the

sea level aquifer is to the east (HDR, 2018). The shallow aquifer is used for private residential water supply, while the sea level and deep aquifers serve as sources of public water supplies for the cities of Lacey, Olympia, and Tumwater (HDR Engineering, Inc. 2017a; Logan et al. 2003). The shallow aquifer near Hawks Prairie is monitored with 21 wells across 2 km^2, and the sea level aquifer is monitored with four wells. The deep aquifer is not monitored in this study, as the effects of MAR on it are thought to be negligible.

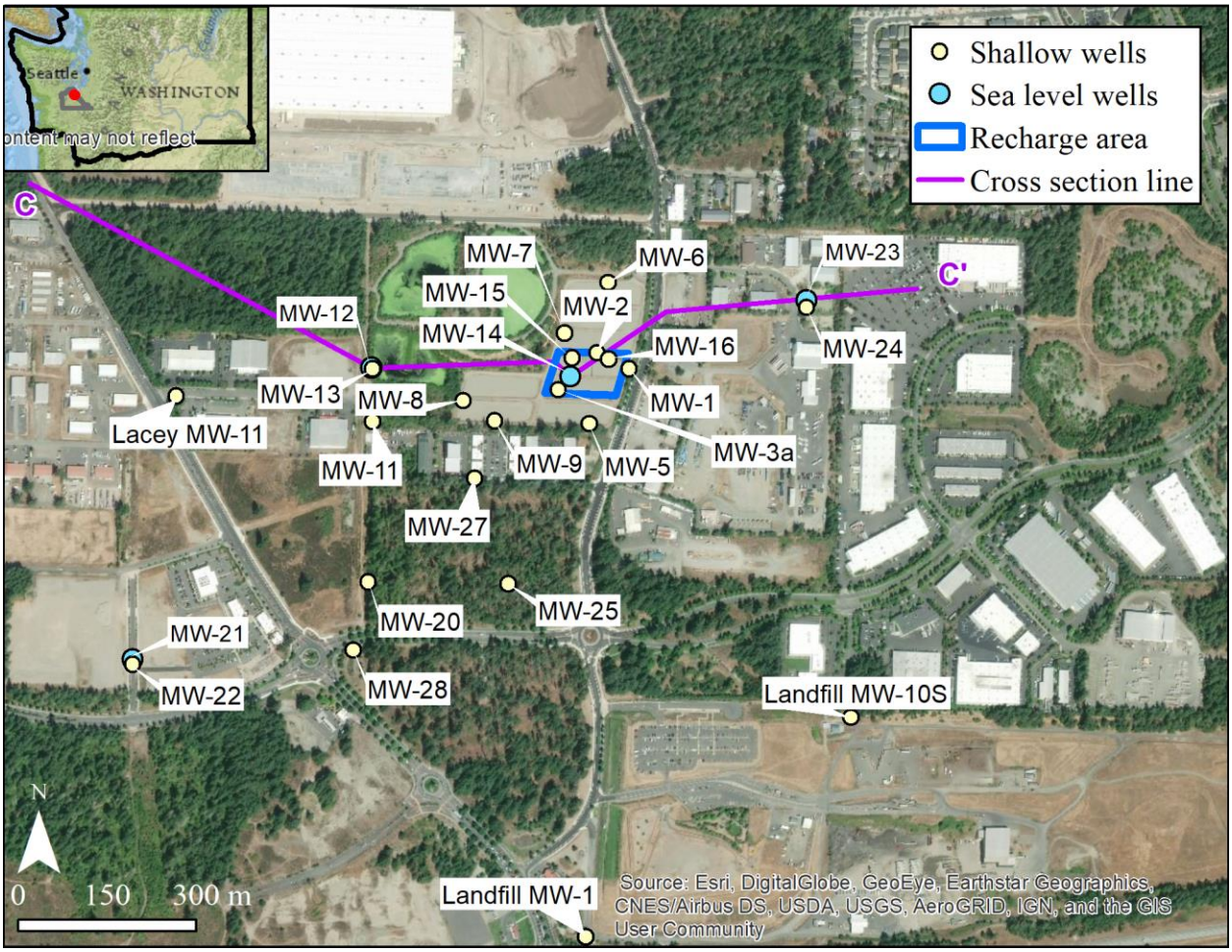

Figure 1: Aerial photo of the Hawks Prairie Facility showing the locations of the basins used for recharge and monitoring wells (MW). Purple line indicates location of cross section shown in

figure 2. Inset map: Washington State outlined in black; Thurston County outlined in gray; study area marked in red.

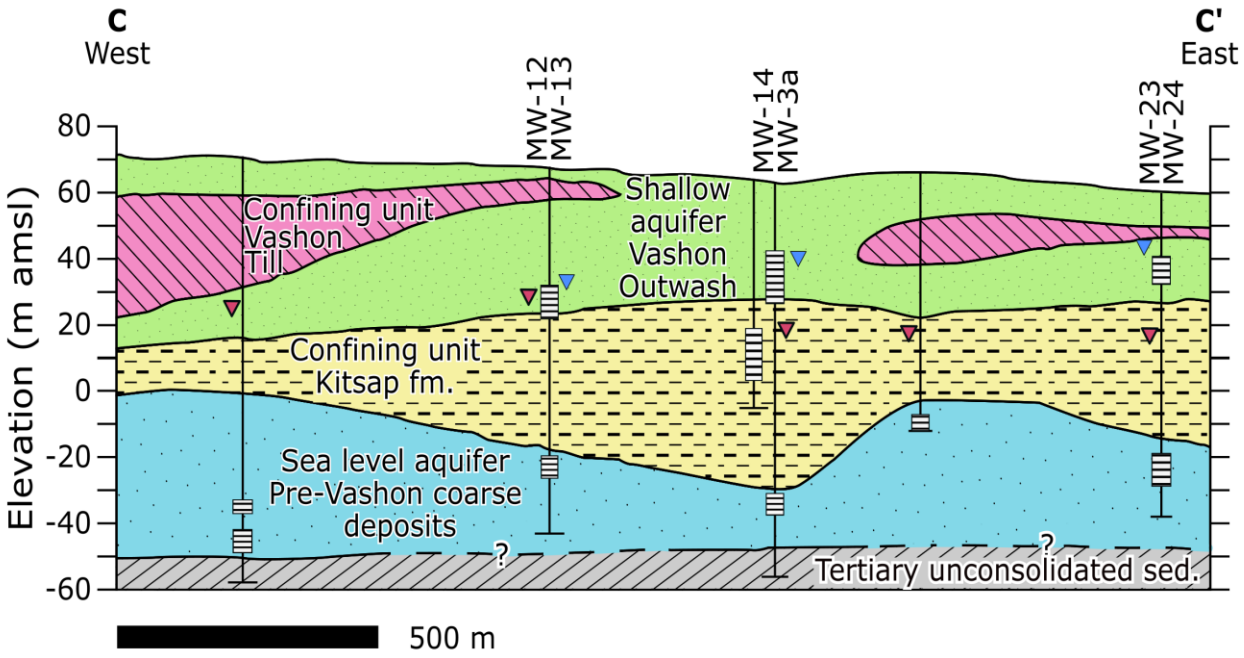

Figure 2: Cross section of study area. Blue triangles denote piezometric surface of the shallow aquifer, as measured during prior hydrogeological characterization, and red, bold edged triangles represent that of the sea level aquifer. Unlabeled wells are preexisting and were not monitored in the study (after HDR Engineering, Inc. 2018).

Theoretical Background

Since SF_6 is a chemically non-reactive gas, it behaves conservatively in saturated aquifers and travels by advection and dispersion at a linear velocity similar to that of the groundwater (Vulava et al. 2002). However, groundwater flow may encounter air in the vadose zone, as well as small, immobile air bubbles that are trapped in aquifers due to water table or pressure fluctuations and remain in gas phase. When dissolved SF_6 encounters trapped air, it exsolves

until its concentration in the air pockets is in equilibrium with the groundwater. Then, it is slowly redissolved as the local SF_6 concentration declines. This exsolution – dissolution process results in the retardation of SF_6, which is the reduction in the velocity of a solute relative to the groundwater's mean linear velocity. This retardation is similar to that caused by sorption and desorption of more reactive compounds (Fry et al. 1995). Ideally, this retardation can be described as a linear function of the aquifer's gas content using the equation

$$R_f = 1 + H * \frac{V_a}{V_w} \quad (1)$$

where R_f is the retardation factor or ratio of the effective velocity of the groundwater to that of the dissolved gas tracer, where V_a and V_w are the volumes of air and water in the aquifer respectively (Fry et al. 1995; Vulava et al. 2002). *H* is the Henry's law constant defined as the equilibrium ratio of the tracer gas concentration in the gas and aqueous phase, which for SF_6 at 12° C is equal to 121 (See appendix A for calculation). This effect has been demonstrated in lab experiments with SF_6, Kr, and ^3H_2O in variously saturated media by Vulava et al. (2002).

The retardation of SF_6 can be calculated from its arrival time at a monitoring well compared to the arrival of a highly soluble and non-reactive tracer such as Br^-. Aquifer saturation is more difficult to measure, and the goal of a tracer study using SF_6 partitioning is to estimate the aquifer's trapped air content. Thus, equ. (1) is rearranged to calculate V_a/ V_w as a function of R_f and *H*.

$$\frac{V_a}{V_w} = \frac{R_f - 1}{H} \quad (2)$$

Using this equation, it is possible to calculate the average degree of saturation between the release and monitoring points using an observed R_f, assuming *H* is known.

Methods

Prior to the experiment, all of the recharge basins were regularly used, saturating most of the underlying porous media. The basins were allowed to drain, and reclaimed water was fed into the northern and southern edges of two of the basins via pipes. A few meters of the basins adjacent to the pipes were inundated to a maximum depth of approximately 10 cm. The remaining area remained dry. From January 16 to February 3, 2018, 2100 kg of potassium bromide (KBr) were dissolved in potable grade water and released into the inflow to the infiltration basins at a rate of 5.5 to 8.2 m^3/d. The Br^- concentration flowing into the basins was measured at 9,800 – 42,500 μg/L. To prepare the SF_6 tracer, 76 L of pure SF_6 and 380 L of water were injected into each of two nylon bags and allowed to equilibrate. Using the equations of Bullister et al. (2002) and assuming ideal gas behavior at a mean air temperature of 6.7 °C, the maximum solubility of SF_6 is 0.459 mmol/L, so about 0.35 mol or 8 L of SF_6 would have gone into solution while the rest remained in the headspace. The equilibrated solution was then added to the recharge water with an average frequency of 1.4 times per day. In total, 207 L (9.0 mol) of SF_6 were added to the recharge water from January 16 to February 2, 2018. Since much of the SF_6 was expected to degas from the infiltration basins before reaching the groundwater, an additional 48 L (2.1 mol) of SF_6 was injected into each of the injection wells: MW-1, MW-2, MW-7, MW-15, and MW-16, between February 7 and 14, 2018. It should be noted that SF_6 is a potent greenhouse gas with the highest greenhouse warming potential named in the IPCC reports; however, the amount used in this study is miniscule compared to the amount used in electrical applications. Furthermore, due to its low mole fraction in the atmosphere, the total radiative forcing due to SF_6 is 0.23% of that of the total CO_2 forcing (Myhre 2013).

During the calendar year 2018, water samples were collected from wells on a daily to weekly basis during January and February, weekly to semimonthly in March, semimonthly in April, and monthly through October. Sampling at MW-1, MW-2, MW-6, and MW-7 was discontinued in late February 2018 following the injection of SF_6 into these wells. Samples tested for bromide were bottled onsite and sent to Eurofins Eaton Analytical for ion chromatography analysis. SF_6 samples were collected in four pre-weighed and sealed 10 mL Vacutainers (blood collection tubes). SF_6 was then analyzed in the headspace of the Vacutainers by gas chromatography equipped with an electron capture detector at University of California, Santa Barbara following the procedure outlined by Clark et al. (2004). At least two replicates must agree within 10% for the measurement to be accepted. The headspace method can be used to analyze water samples containing SF_6 at concentrations ranging from 0.05 pmol/L to 23.6 nmol/L (23,600 pmol/L). In samples with SF_6 concentrations exceeding what can be measured by the headspace method, a small quantity of the equilibrated solution, which has a lower concentration than what was originally sampled due to Henry's law exsolution, can be transferred to a new container for measurement and the initial concentration calculated (See appendix A).

Average velocity from basin to well is determined by dividing the direct distance from the edge of the nearest infiltration basin to the well screen by travel time. Travel time is calculated starting with the date on which 50% of each tracer had been added to the infiltrating water and ending with the arrival of the peak tracer concentration or tracer center of mass (COM), which is determined by integrating under the breakthrough curve. COM can only be accurately determined for complete breakthrough curves, while the peaks can be identified when concentrations start to decline, even if they have not returned to background levels.

Results

Tracer concentrations were measured in monitoring wells from January to October 2018, and breakthrough curves are available for several wells (Fig. 3-6). Following the beginning of infiltration, both tracers were first detected above background levels at MW-5 in the shallow aquifer. Both tracers exhibit distinctive double peaks in the breakthrough curve at this well in January to early February (Fig. 3). In the case of Br^-, the tracer patch then spread predominately to the west and additionally to the north and south (Fig. 7). High Br^- levels were measured in shallow wells MW-3a and MW-16 in late January, but concentrations above background level were not detected at nearby MW-15 until late March and were not detected at MW-2. The SF_6 injected into wells MW-1, MW-2, MW-7, MW-15, and MW-16 in early February quickly overshadowed the signature from SF_6 infiltration observed in MW-5. The SF_6 migrated downgradient in a southwesterly direction, but concentrations at MW-3a remained low relative to nearby MW-5 and to downgradient MW-8, MW-9, and MW-27 until late March (Fig. 4 and 8). The farthest that SF_6 spread during the study period was to MW-13 and MW-27, approximately 300 m downgradient in the shallow aquifer (Fig. 8). With the exception of MW-12 which has breakthroughs occurring at similar times to its nested partner MW-13, detections in the sea level aquifer were small and isolated (Fig. 5).

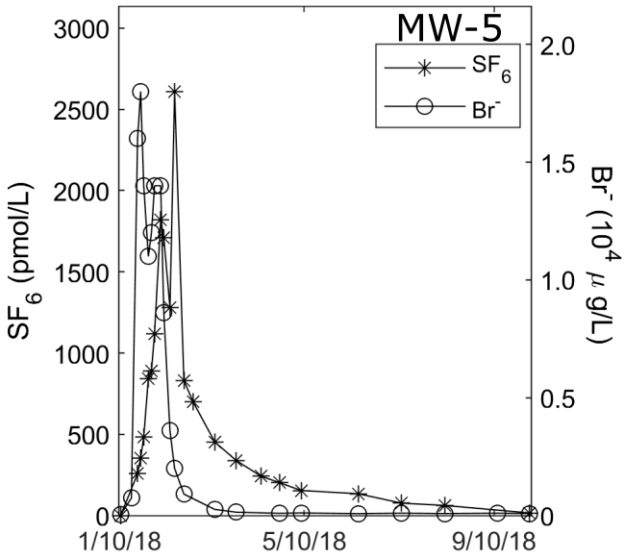

Figure 3: Breakthrough curve at MW-5 showing double peaks for both tracers.

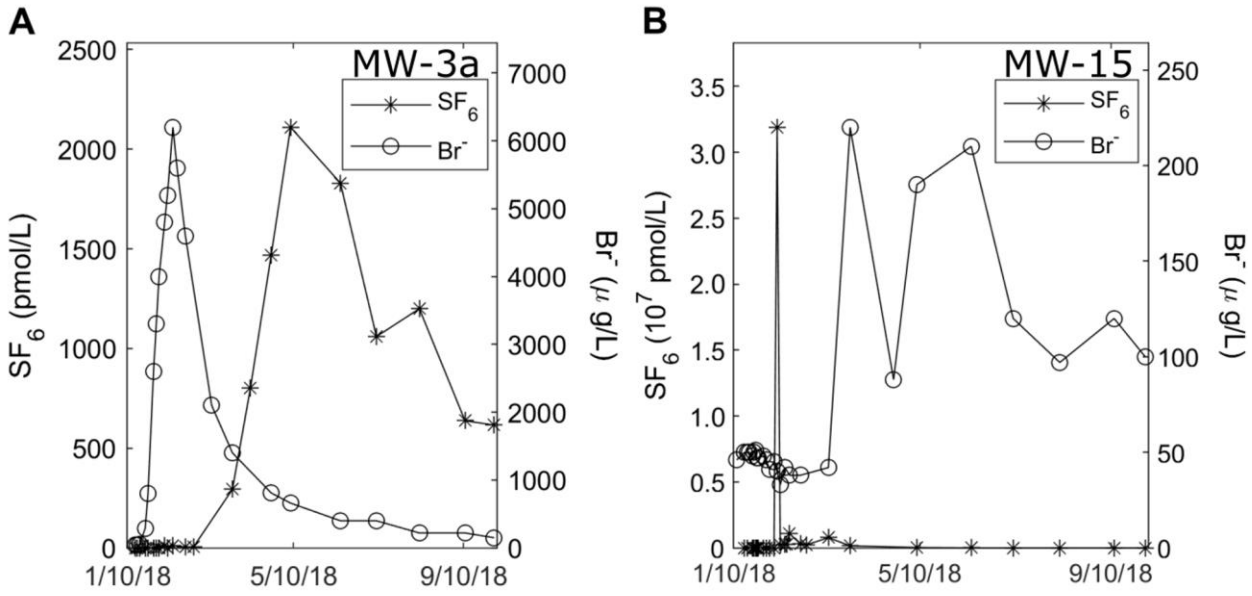

Figure 4: Breakthrough curves for (A) MW-3a and (B) MW-15. Note that Br^- at MW-3a significantly precedes that at MW-15, while SF_6, which was added directly to MW-15, is late to

arrive at MW-3a.

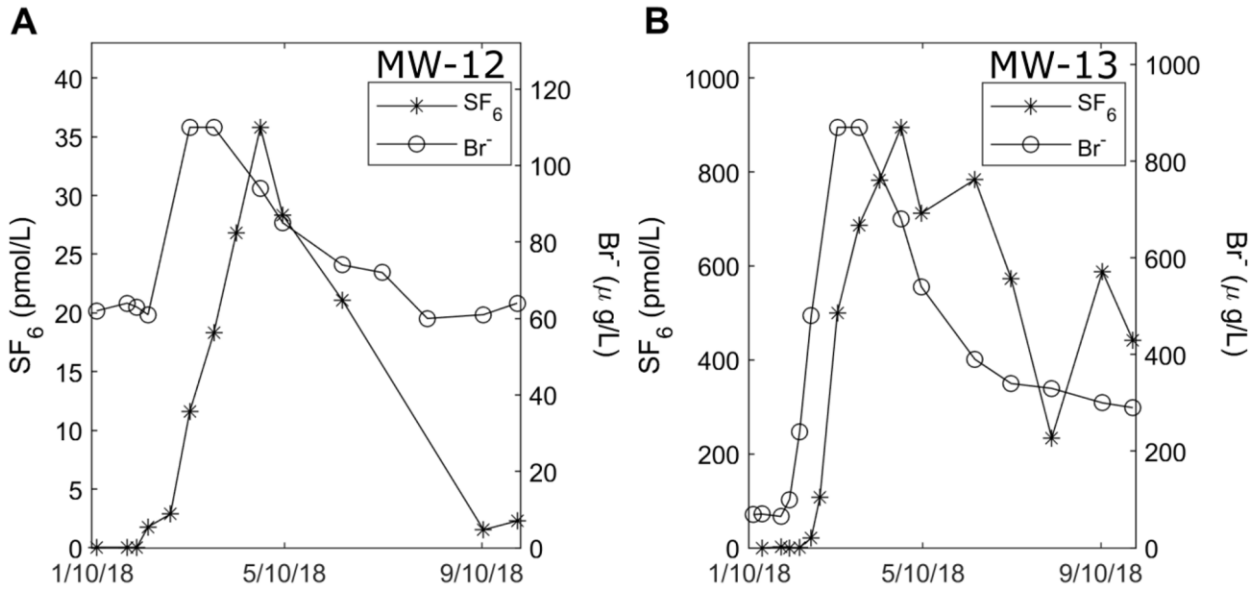

Figure 5: Breakthrough curves for (A) MW-12 and (B) MW-13. Arrivals of both tracers at MW-12 follow those at MW-13 closely even though MW-12 is screened in the sea level aquifer and MW-13 is screened in the shallow.

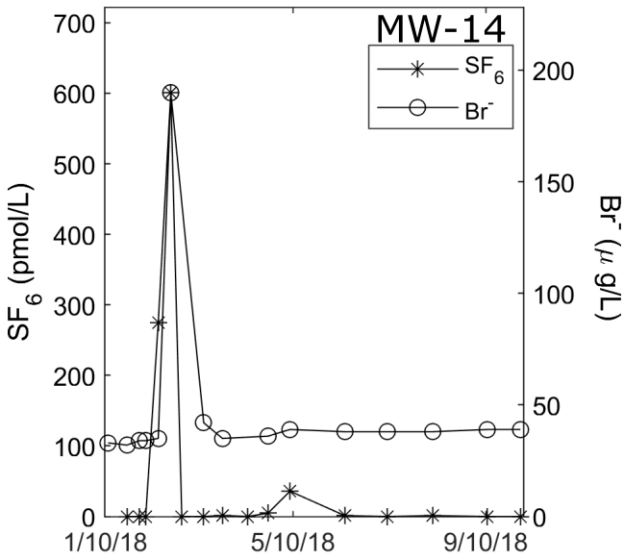

Figure 6: Breakthrough curve for MW-14 showing isolated spikes of both tracers.

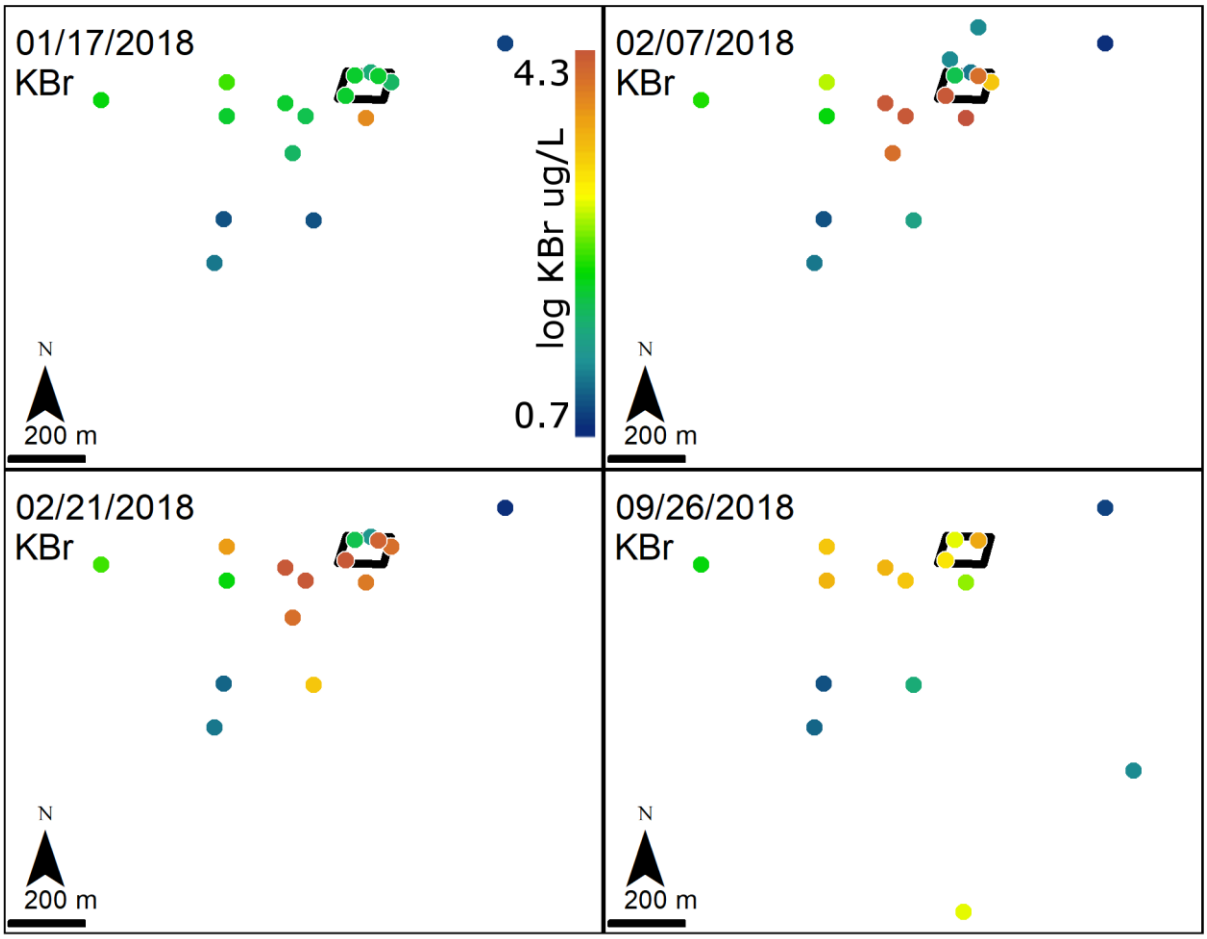

Figure 7: Br^- concentration measured in shallow aquifer monitoring wells with infiltration basins outlined in black. Color scale is the same for all dates. Br^- first appears in MW-5, shown on January 31st in orange, to the south of the basins. Br^-, which unlike SF_6 was not injected into any wells, is low in February at MW-2 and MW-15 relative to surrounding wells. By September, Br^- concentrations are representative of the end of the monitoring period.

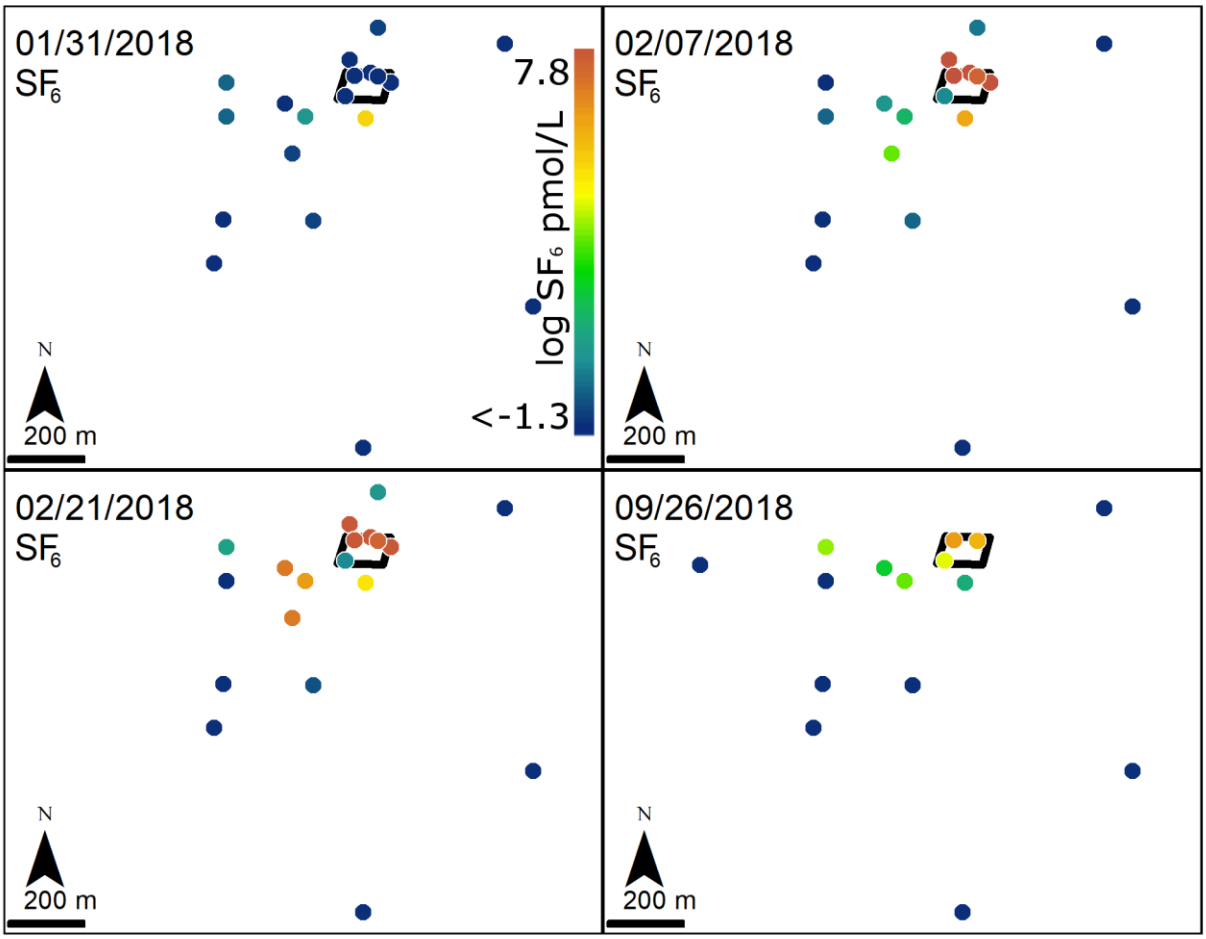

Figure 8: Like Br^-, SF_6 is first detected at MW-5, though at a later date. High concentrations can be observed in injection wells indicated in red along the north edge of the basins on February 7th. Concentrations remain low at MW-3a in the southwest corner of the basins, despite being surrounded by wells with higher concentrations. Concentrations in September are representative of the end of the monitoring period.

In monitoring wells where arrivals of both tracers can be detected, Br^- precedes SF_6. The exception to this is MW-14, where detections of both tracers are questionable due to their brevity (Fig. 6). In wells where tracer concentrations have begun to decline, the peak concentration are used to approximate the mean velocity of the tracer arriving at that well (Fig. 9). Among the

wells where both tracers have peaked, SF_6 has peaked later than Br^- in all but MW-14, where the peaks arrived on the same date. If a breakthrough curve is relatively complete, its mean velocity can be more accurately determined from its COM. Eight monitoring wells have sufficiently complete breakthrough curves to approximate a COM for both tracers, all of which except for MW-14 and MW-27 show retardation of SF_6 relative to Br^-. Injection wells are excluded from tracer velocity analysis.

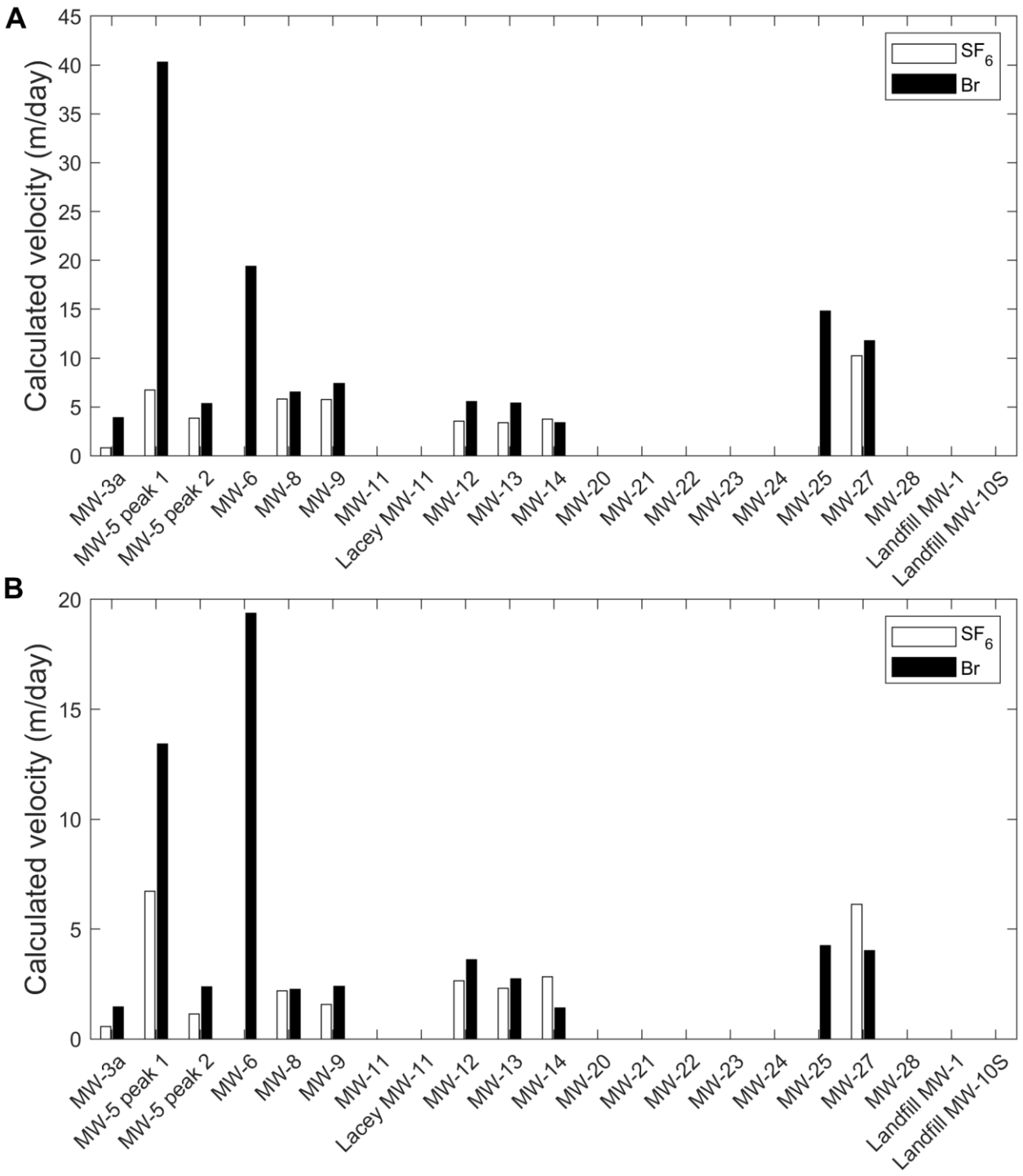

Figure 9: Mean linear tracer velocities estimated from (A) peak and (B) center of mass arrivals. Only those wells with complete enough break through curves to identify a peak or approximate a center of mass are shown.

Since Br^- travels at the same velocity as the groundwater and both tracers can be assumed to reach a well by the same flow paths, the average retardation of SF_6 along the flow path that it takes to reach the well can be determined by dividing the arrival time of SF_6 by that of Br^- (Fig. 10). The average retardation across the study site determined from peak arrivals is 2.2±3.5. For the shallow aquifer only, the average retardation is 2.5±3.8. Using COM, average retardation is 1.4±1.3 or 1.6±1.2 for the shallow aquifer only (Table 1).

Table 1: Arrival times and retardation factors by well.

Well		Distance (m)	$t_{peak\ SF6}$ (days)	$t_{peak\ Br-}$ (days)	Peak retardation	$t_{COM\ SF6}$ (days)	$t_{COM\ Br-}$ (days)	COM retardation
MW-3a		82	103	21	4.90	142	56	2.54
MW-5	peak 1	81	12	2	6.00	12	6	2.00
	peak 2	81	21	15	1.40	70	34	2.06
MW-6		155	-	8	-	-	8	-
MW-8		156	27	24	1.13	71	69	1.03
MW-9		155	27	21	1.29	99	65	1.52
MW-11		308	-	-	-	-	-	-
Lacey MW-11		763	-	-	-	-	-	-
MW-12		318	90	57	1.58	120	88	1.36
MW-13		308	90	57	1.58	133	112	1.19
MW-14		102	27	30	0.90	36	72	0.50
MW-20		459	-	-	-	-	-	-
MW-21		826	-	-	-	-	-	-
MW-22		1067	-	-	-	-	-	-
MW-23		316	47	-	-	-	-	-
MW-24		306	12	-	-	-	-	-
MW-25		459	-	31	-	-	109	-
MW-27		307	30	26	1.15	50	76	0.66
MW-28		611	-	-	-	-	-	-
Landfill MW-1		764	-	-	-	-	-	-
Landfill MW-10S		1068	-	-	-	-	-	-

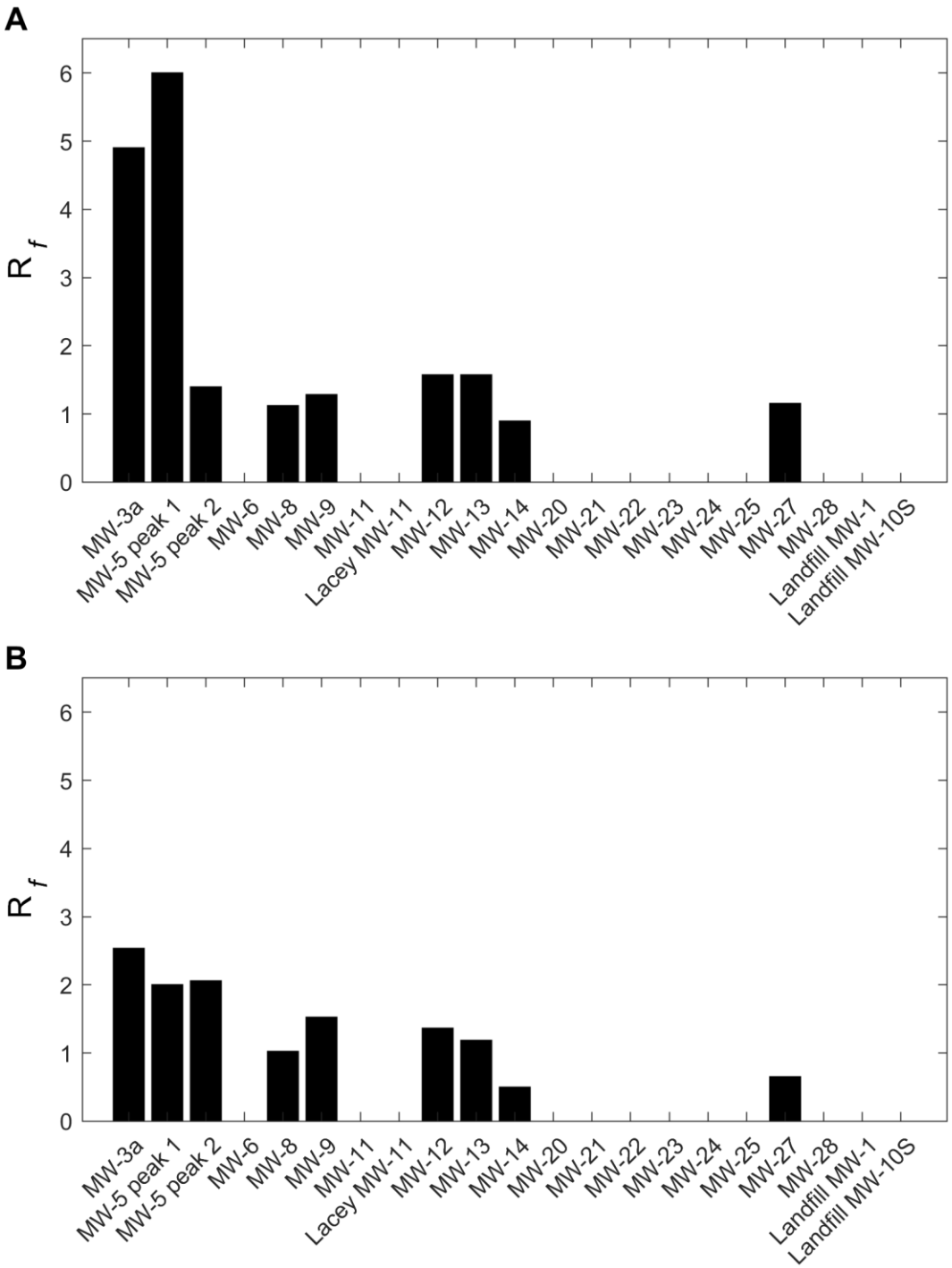

Figure 10: Retardation of SF_6 relative to Br^- (assumed to travel at the same velocity as groundwater) based on (A) peak and (B) center of mass arrivals. An R_f value of 1 indicates no retardation, while an R_f greater than one indicates that the SF_6 has been slowed.

Discussion

COM arrivals are considered a more reliable measure of tracer velocity than peak arrivals, as they take into account breakthrough curve asymmetry. However, measurements at the site were terminated due to budget constraints before tracers at most wells returned to background concentrations. Thus, the COM times should be considered minimums and velocities calculated from them maximums. Both methods suggest moderate retardation of SF_6 to varying degrees along different flow paths to wells. The variation in retardations calculated at different wells indicates that trapped air is distributed heterogeneously across the Hawks Prairie site. Hydraulic conductivity also seems to be heterogeneous, given the extremely broad range in flow velocities along different flow paths and the disparities between tracer levels at wells such as MW-15 and MW-3a. Drilling logs indicate that Vashon Till is interfingered with the Vashon outwash below the infiltration basins. It is possible that the till is acting locally as a barrier to shallow flow beneath the basins. The arrival of the tracers at MW-5 above background concentrations before the wells in the infiltration basins suggests a preferential pathway to MW-5 and possibly effects of differential saturation within the basins. Its unique double peak may be indicative of two separate flow paths leading to the well as discussed by McDermott et al. (2008). Since two adjacent basins were used for recharge and were only inundated on the northern and southern edges, it is also possible that the first set of peaks represents arrival of tracers from the nearer basin and the second set from the farther one. The breakthrough curve for each tracer was separated into two single peak curves (appendix B) for analysis, and the first peak was found to exhibit significantly greater retardation than the second. This suggests that there is more trapped air along the first flow path. Applying equation (2) to the calculated retardations provides an estimated ratio of trapped air to groundwater along each flow path

(Table 2). Flow paths for which $R_f \leq 1$ are assumed to have no trapped air. Pore space air to water ratios are calculated in the 10^{-3} to 10^{-2} range (Fig. 11).

Table 2: Trapped air to water ratios along flow paths to each well calculated with equ. (2), assuming a temperature of 12° C.

Well		V_a/V_w (peak)	V_a/V_w (COM)
MW-3a		0.0323	0.0127
MW-5	peak 1	0.0413	0.0083
	peak 2	0.0033	0.0088
MW-6		-	-
MW-8		0.0010	0.0002
MW-9		0.0024	0.0043
MW-11		-	-
Lacey MW-11		-	-
MW-12		0.0048	0.0030
MW-13		0.0048	0.0015
MW-14		0	0
MW-20		-	-
MW-21		-	-
MW-22		-	-
MW-23		-	-
MW-24		-	-
MW-25		-	-
MW-27		0.0013	0
MW-28		-	-
Landfill MW-1		-	-
Landfill MW-10S		-	-

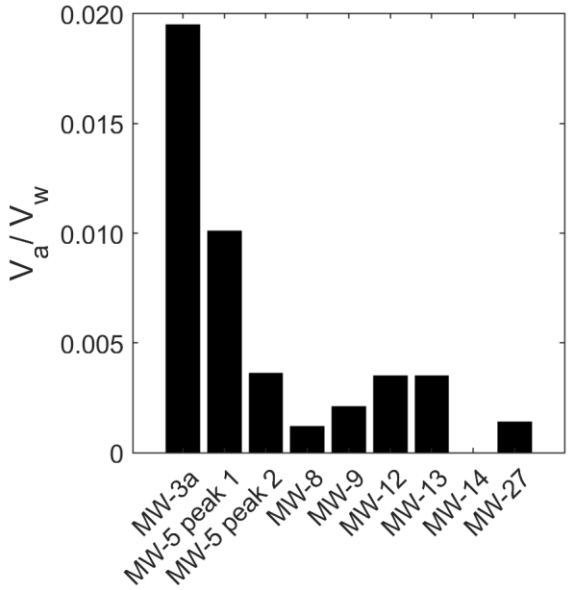

Figure 11: Trapped air to water ratios encountered along paths to wells in pore space calculated from peak arrival time ratios. Trapped air quantities are small but variable between paths.

Based on the hydraulic gradient, HDR (2017b) divided the shallow aquifer into two zones. Zone 1, which is located northeast of MW-20, has a horizontal hydraulic gradient of 0.023, while zone 2, which is located southwest of MW-20 has gradient of 0.002. Water recharged at the basins must travel through zone 1 to reach zone 2. Slug and pump tests suggest a hydraulic conductivity of 30 – 60 m/d, and effective porosity has been estimated at 0.18 – 0.25 (HDR Engineering, Inc. 2017b; Truex et al. 2011). Using Darcy's law, this yields an expected linear velocity in the shallow aquifer of 2.8 – 7.7 m/d in zone 1 and 0.24 – 0.67 m/d in zone 2. Previous measurements of temperature and salinity changes in response to recharge at the site yield a velocity of 4.0 – 13 m/d (HDR Engineering, Inc. 2017b). Given that groundwater must travel through the much slower zone 2 to arrive at wells MW-22, MW-28 and Landfill MW-1, it is not surprising that there were no confirmed tracer detections at these wells (Table 3). Calculated linear velocities in zone 1 are highly variable, suggesting that flow paths differ

considerably in conductivity and sinuosity (Table 4). The majority of wells with detections of Br^- exhibited velocities in the previously measured range, though MW-6, MW-25, and most dramatically, the first peak of MW-5 were higher. Meanwhile, MW-11, MW-20, and MW-24 had no detections during the monitoring period, even though they are close enough for recharge water to reach if it were traveling at least at the minimum calculated velocity. Velocities calculated from tracer centers of mass are slower than those calculated from peaks due to the asymmetric shapes of the breakthrough curves (Table 5).

Table 3: Distances to zone 2 wells, separated into distances which must be travelled through zone 1 and distances which must subsequently be travelled in zone 2 along the most direct path from basin to well. None of these wells saw tracer detections during the monitoring period, so the maximum possible velocity that would not result in a detection is compared with the expected velocity.

Well	Zone 1 distance (m)	Zone 2 distance (m)	Comparison to expected velocity
MW-22	480	587	Undetermined
MW-28	425	186	Lower
Landfill MW-1	470	294	Undetermined

Table 4: Br^- velocities from peak arrivals at zone 1 wells compared to calculated and previously measured groundwater velocity ranges. Wells with no breakthrough are determined to have lower than expected velocities if linear travel at the minimum expected velocity would have brought the tracer to the well by the last measurement date.

Well		Distance (m)	Br^- velocity (m/d)	Comparison to expected velocity
MW-3a		82	3.9	Calculated range
MW-5	peak 1	81	40	Higher
	peak 2	81	5.4	Both ranges
MW-6		155	19	Higher
MW-8		156	6.5	Both ranges
MW-9		155	7.4	Previous range
MW-11		308	-	Lower
Lacey MW-11		763	-	Undetermined

MW-13	308	5.4	Both ranges
MW-20	459	-	Lower
MW-24	306	-	Lower
MW-25	459	15	Higher
MW-27	307	12	Previous range
Landfill MW-10S	1068	-	Undetermined

Table 5: Br^- velocities from center of mass arrivals at zone 1 wells compared to calculated and previously measured groundwater velocity ranges as in Table 4.

Well		Distance (m)	Br^- velocity (m/d)	Comparison to expected velocity
MW-3a		82	1	Lower
MW-5	peak 1	81	13.4	Higher
	peak 2	81	2.4	Lower
MW-6		155	19	Higher
MW-8		156	2.3	Lower
MW-9		155	2.4	Lower
MW-11		308	-	Lower
Lacey MW-11		763	-	Undetermined
MW-13		308	2.7	Lower
MW-20		459	-	Lower
MW-24		306	-	Lower
MW-25		459	4.2	Both ranges
MW-27		307	4.0	Both ranges
Landfill MW-10S		1068	-	Undetermined

Prior measurements indicate a vertical gradient of -0.09 to -0.45 between the shallow and sea level aquifers, which would suggest a less permeable confining layer throughout most of the study site than the breakthrough at MW-12 appears to indicate. (HDR Engineering, Inc. 2017b). Given that the breakthrough at MW-12 seems to approximately coincide with that at MW-13, with which it is nested, it is likely that there is preferential pathway through the Kitsap Formation nearby. The apparently identical retardations calculated from the two wells' peak

arrivals also suggest that groundwater travelling to the two wells follows very similar flow paths, since it appears to encounter similar amounts of trapped air. Additionally, since MW-12 is upgradient of recharge in the sea level aquifer, it is far more feasible for the tracer to have travelled most of the way in the shallow aquifer than for it to have travelled primarily in the sea level aquifer. Among the other sea level wells, only MW-14 has both SF_6 and Br^- detections at similar times, and these only occur for one or two measurements. This suggests that the majority of detections at sea level wells are either false positives or the result of minor, intermittent transmission of water.

The sea level aquifer has a hydrologic gradient of 0.01 with groundwater flowing eastward. Its hydraulic conductivity as determined from slug and pump tests is 0.6 – 12 m/d (HDR Engineering, Inc. 2017b). If it is assumed to have a similar effective porosity to the shallow aquifer, then the resulting groundwater velocity would be 0.03 – 0.67 m/d. Given that any tracer arriving at a well screened in the sea level aquifer would have to first travel down through the confining layer, the mean velocity along the entire flow path should be even slower. MW-12 and possibly MW-14 are the only sea level wells with reliable detections and have mean Br^- velocities of 5.6 and 3.4 m/d respectively. These velocities are an order of magnitude higher than predicted, lending credence to the idea that any water traveling from the surface to the sea level aquifer must follow preferential pathways.

Conclusion

The application of SF_6 and Br^- as groundwater tracers at the Hawks Prairie site in Thurston County, Washington demonstrates how the use of paired gas and ionic tracers can reveal the distribution of trapped air in the subsurface. Flow velocity in the shallow aquifer ranges from 3.9 to 40 m/d. Water flow velocities and concentration disparities between nearby

wells suggest that groundwater at the site follows several non-linear flow paths. Retardation of SF_6 relative to Br^- was observed at most wells, indicating partitioning of the gas tracer into trapped air. Average retardation of SF_6 in the shallow aquifer based on peak arrivals was 2.5±3.8, reflecting differing trapped air contents along different flow paths. Connection between the shallow and sea level aquifers is highly localized and largely intermittent.

Acknowledgement

Thanks to the LOTT Clean Water Alliance for providing access to the study site and funding for this study. Thanks to HDR Engineering, Inc. for logistical work. The authors would also like to thank the two anonymous reviewers for their comments which improved the manuscript.

References

Balcke, G.U., S. Meenken, C. Hoefer, and S.E. Oswald. 2007. "Kinetic Gas-Water Transfer and Gas Accumulation in Porous Media during Pulsed Oxygen Sparging." *Environmental Science and Technology* 41 (12): 4428–34.

Bouwer, H. 2002. "Artificial Recharge of Groundwater: Hydrogeology and Engineering." *Hydrogeology Journal* 10 (1): 121–42.

Bullister, J.L., D.P. Wisegarver, and F.A. Menzia. 2002. "The Solubility of Sulfur Hexafluoride in Water and Seawater." *Deep-Sea Research Part I: Oceanographic Research Papers* 49 (1): 175–87.

Christiansen, J.E. (USDA). 1944. "Effect of Entrapped Air upon the Permeability of Soils." *Soil Science* 58 (5): 355–65.

Clark, J.F., G.B. Hudson, and D. Avisar. 2005. "Gas Transport below Artificial Recharge Ponds:

Insights from Dissolved Noble Gases and a Dual Gas (SF6 and 3He) Tracer Experiment." *Environmental Science and Technology* 39 (11): 3939–45.

Clark, J.F., G.B. Hudson, M.L. Davisson, G. Woodside, and R. Herndon. 2004. "Geochemical Imaging of Flow Near an Artificial Recharge Facility, Orange County, California." *Ground Water* 42 (2): 167–74.

Dillon, K.S., D.R. Corbett, J.P. Chanton, W.C. Burnett, and D.J. Furbish. 1999. "The Use of Sulfur Hexafluoride (SF_6) as a Tracer of Septic Tank Effluent in the Florida Keys." *Journal of Hydrology* 220 (3-4): 129–40.

Dillon, P. 2005. "Future Management of Aquifer Recharge." *Hydrogeology Journal* 13 (1): 313–16.

Flury, M. and N. N. Wai. 2003. "Dyes as tracers for vadose zone Hydrology" *Reviews in Geophysics* 41(1): 1002.

Fry, V.A., J.D. Istok, L. Semprini, K.T. O'Reilly, and T.E. Buscheck. 1995. "Retardation of Dissolved Oxygen Due to a Trapped Gas Phase in Porous Media." *Groundwater* 33 (3): 391–98.

HDR Engineering Inc. 2017a. "LOTT Clean Water Alliance Reclaimed Water Infiltration Study: Groundwater Quality Characterization (Task 1.1) Technical Memorandum."

———. 2017b. "LOTT Clean Water Alliance Reclaimed Water Infiltration Study: Hydrogeologic Characterization Report- On-Site Wells and Lysimeter Installation (Task 2.1.1.A), Off-Site Monitoring Wells (Task 2.1.2.C)."

———. 2018. "LOTT Clean Water Alliance Reclaimed Water Infiltration Study Work Plan:

Tracer Testing and Water Quality Monitoring of Treatment Effectiveness (Task 2.1.3)."

Heilweil, V.M., D.K. Solomon, K.S. Perkins, and K.M. Ellett. 2004. "Gas-Partitioning Tracer Test to Quantify Trapped Gas during Recharge." *Groundwater* 42 (4): 589–600.

Logan, R.L., T.J. Walsh, H.W. Schasse, and M. Polenz. 2003. "Geologic Map of the Lacey 7.5-Minute Quadrangle, Thurston County, Washington." Washington State Department of Natural Resources, Washington Division of Geology and Earth Resources open file report 2003-9.

McDermott, J.A., D. Avisar, T.A. Johnson, and J.F. Clark. 2008. "Groundwater Travel Times near Spreading Ponds: Inferences from Geochemical and Physical Approaches." *Journal of Hydrologic Engineering* 13 (11): 1021–28.

Myhre, G., D. Shindell, F.-M. Breon, W. Collins, J. Fuglestvedt, J. Huang, D. Koch, et al. 2013. "Anthropogenic and Natural Radiative Forcing." In *Climate Change 2013 the Physical Science Basis: Working Group I Contribution to the Fifth Assessment Report of the Intergovernmental Panel on Climate Change*, edited by T. F. Stocker, D. Qin, G.-K. Plattner, M. Tignor, S. K. Allen, J. Boschung, A. Nauels, Y. Xia, V. Bex, and P. M. Midgley, 659–740. Cambridge, United Kingdom and New York, NY, USA: Cambridge University Press.

Truex, M.J., V.R. Vermeul, D.P. Mendoza, B.G. Fritz, R.D. Mackley, M. Oostrom, T.W. Wietsma, and T.W. Macbeth. 2011. "Water Level Monitoring Pressure Transducers : A Need for Industry-Wide Standards." *Ground Water Monitoring & Remediation* 31 (1): 50–58.

Vulava, V.M., E.B. Perry, C.S. Romanek, and J.C. Seaman. 2002. "Dissolved Gases as

Partitioning Tracers for Determination of Hydrogeological Parameters" 36 (2): 254–62.

Wanninkhof, R., J.R. Ledwell, W.S. Broecker, and M. Hamilton. 1987. "Gas Exchange on Mono Lake and Crowley Lake, California." *Journal of Geophysical Research: Oceans* 92 (C13): 14567–80.

Supporting information

Appendix S1: Derivation of water transfer equations

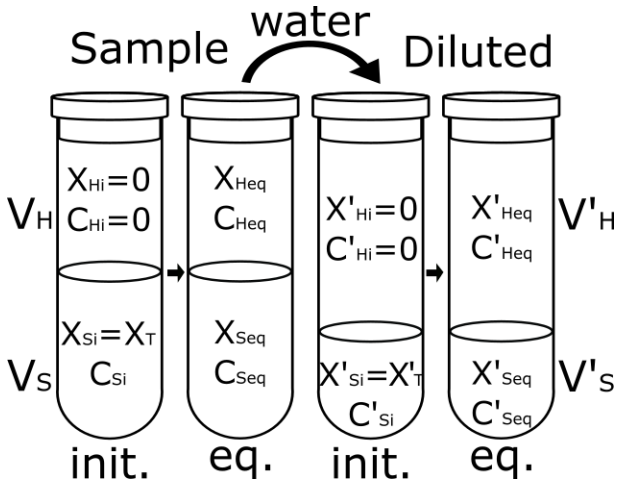

Figure S1.1: Illustration of water transfer showing parameters associated with each step.

In samples with SF_6 concentrations exceeding what can be measured by the headspace method (> 23.6 nmol/L), a small quantity of the equilibrated solution in the original container can be transferred to a new container (Fig. S1.1). The transferred solution has a lower concentration than what was originally injected to the first container, so when the second container reaches equilibrium, the solution and headspace concentrations are much lower. For instance, if a Vacutainer contains equal volumes of sample and headspace, the ratio of equilibrium to initial concentration of SF_6 in solution will be

$$\frac{C_{Seq}}{C_{Si}} = \frac{1}{H+1} \quad \text{(S1.1)}$$

Where C_s is the concentration in solution initially (C_{si}) and at equilibrium (C_{Seq}), and *H* is the Henry's law coefficient.

By starting with the lower, equilibrium concentration of the solution from the first container, the headspace concentration in the second container is more likely to fall within the measurable range. The initial concentration of the original solution can then be calculated from the headspace concentration of the new container as follows:

In each container, the total amount of SF_6 in moles, denoted X, will be divided between the solution and the headspace according to Henry's Law such that:

$$X_T = X_S + X_H \quad \text{(S1.2)}$$

Because all of the SF_6 starts in the solution:

$$X_T = X_{Si} \quad \text{(S1.3)}$$

The number of moles in a given phase is equal to its volume V multiplied by concentration C.

$$X_S = V_S C_S \text{ and } X_H = V_H C_H \quad \text{(S1.4)}$$

According to Henry's Law, the headspace and solution concentrations at equilibrium are related to each other by the Henry's Law coefficient, *H*:

$$H = \frac{C_{Heq}}{C_{Seq}} \tag{S1.5}$$

Multiplying both sides by the volume ratio makes them equal to the equilibrium mole ratio.

$$H\frac{V_H}{V_S} = \frac{V_H C_{Heq}}{V_S C_{Seq}} \tag{S1.6}$$

Combining equations (S1.2), (S1.3), (S1.4), and (S1.6) at equilibrium:

$$H\frac{V_H}{V_S} = \frac{V_H C_{Heq}}{V_s C_{Si} - V_H C_{Heq}} \tag{S1.7}$$

Solve for C_{Si}.

$$C_{Si} = \frac{C_{Heq}(HV_H + V_S)}{HV_S} \tag{S1.8}$$

When C_{Heq} is measured in a new container after a portion of the original solution has been transferred and allowed to equilibrate, then H is H', the equilibrium ratio the when the measurement was taken in the second container, and C_{Si} is C'_{si}, the concentration of the solution when it was transferred. Thus, the equation can be re-written:

$$C'_{Si} = \frac{C'_{Heq}(H'V'_H + V'_S)}{H'V'_S} \tag{S1.9}$$

Equation (S1.9) provides the initial concentration of the solution in the new container. To calculate the initial concentration in the original container, once again equations (S1.2), (S1.3), (S1.4), and (S1.6) are combined and solved for C_{Si} using C_{Seq} instead of C_{Heq}.

$$H\frac{V_H}{V_S} = \frac{V_s C_{Si} - V_S C_{Seq}}{V_S C_{Seq}} \tag{S1.10}$$

Solve for C_{Si}.

$$C_{Si} = \frac{C_{Seq}(HV_H + V_S)}{V_S} \tag{S1.11}$$

In our case, C_{Seq} is C'_{Si}, and *H* refers to when the solution was equilibrated in the first container and transferred to the new one, so the equation becomes:

$$C_{Si} = \frac{C'_{Si}(HV_H + V_S)}{V_S} \tag{S1.12}$$

Because the dry air mole fraction *x*, not C_H is directly measured, and that the quantity of solution is more accurately measured as mass, equations (S1.9) and (S1.12) become:

$$C'_{Si} = \frac{x\left(H'_{grav}V'_H\rho_{N2} + m'_S\right)}{H'_{grav}M_{N2}m'_S} \tag{S1.13}$$

and

$$C_{Si} = \frac{C'_{Si}\left(H_{grav} V_H \rho_{N2} + m_S\right)}{m_S} \quad \text{(S1.14)}$$

It is important to note that the *H* values used in equations (S1.13) and (S1.14) are gravimetric, as opposed to the volumetric values used in prior equations. In order to determine *H*, it is helpful to use a parameter that Weiss and Price (1980) define as F, where:

$$F = \frac{C_{Seq}}{x} \quad \text{(S1.15)}$$

Using the parameters determined by Bullister et al. (2002), the F for SF_6 in fresh water can be determined as a function of absolute temperature T with the following equation:

$$\ln F = -82.1639\ mol/(kg\ atm) + 120.152\ mol/(kg\ atm)\ (100/T) + 30.6372\ mol/(kg\ atm)\ \ln (T/100) \quad \text{(S1.16)}$$

A gravimetric *H* is obtained by substituting equation (S1.15) into equation (S1.5) where total pressure P is assumed to equal 1 atm and M_{N2} is the molar mass for nitrogen gas (14 mol/g).

$$H_{grav} = 1 / (F\ P * M_{N2}) \quad \text{(S1.17)}$$

Combining the water transfer method with the headspace method allows water samples containing SF_6 up to 64 μmol/L to be analyzed. Out of 379 accepted SF_6 concentration data points used in this study, 31 were measured with water transfers.

Variables

C	concentration
C_{Heq}	concentration in headspace at equilibrium
C_{Seq}	concentration in solution at equilibrium
C_{Si}	initial concentration in solution (sample concentration)
F	equilibrium ratio of solution concentration to headspace dry air mole fraction
H	Henry's Law constant
H_{grav}	Henry's Law constant (gravitational)
M_{N2}	molar mass of nitrogen gas (28.0134 g/mol)
m_S	mass of solution
P	total pressure
T	absolute temperature (Kelvin)
V	volume
V_H	headspace volume
V_S	solution volume
X	number of moles
X_H	number of moles in headspace
X_S	number of moles in solution
X_T	total number of moles in container
x	dry air mole fraction of SF_6 in headspace
ρ_{N2}	density of nitrogen gas (1.250 g/L at STP)

An apostrophe following any variable (e.g. V'_H) indicates that it refers to the second container.

Appendix S2: Separation of double peaked breakthrough curves

The double peak in both tracers observed at MW-5 is assumed to represent two distinct flow paths to that well. In order to separate the signatures of the two paths, the breakthrough curve for each tracer was broken into two curves. Clearly defined breakthrough curves observed in other wells were fitted for linear and first order exponential decline from their peaks, and exponential decay was determined to provide a better representation of the decline in tracer concentrations based on greater R^2 values (Table S2.1).

Table S2.1: R^2 values for linear and exponential fits of the decline in tracer concentrations following peaks in observed, clearly defined breakthrough curves. Note that MW-5 refers to the measured decline from the second peak.

	Well	Linear R^2	Exponential R^2
Br^-	MW-3a	0.6271	0.9897
	MW-5	0.2821	0.998
	MW-8	0.7131	0.9886
	MW-9	0.6579	0.9801
SF_6	MW-5	0.3573	0.9059
	MW-8	0.4067	0.9628
	MW-9	0.2775	0.8115
	MW-16	0.3858	0.9943
	MW-27	0.6414	0.9913

At MW-5, the first curve was assumed to be identical to the observed breakthrough curve until the first peak. Following the peak, the first curve was assumed to decline by first order exponential decay, like the other breakthrough curves. The second curve was calculated as the difference between the observed breakthrough curve and the estimated curve for peak 1. Thus, the two curves together produce the observed breakthrough curve (Fig. S2.1-S2.2). A decay constant of -0.15 was determined to produce the most realistic curves for MW-5, such that the decay equation following the first peak of either tracer can be written as

$$C = C_{peak}\, e^{-0.15\,(t - t_{peak})} \qquad \text{(S2.1)}$$

Peak and center of mass arrival times were then determined for each of the separated curves.

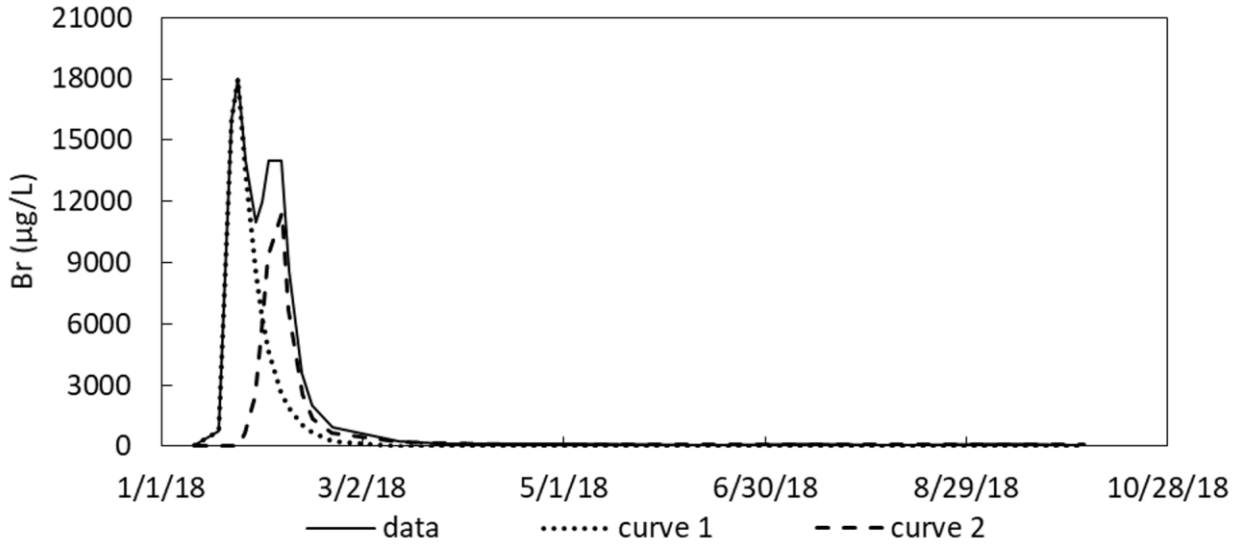

Figure S2.1: Br breakthrough curve at MW-5 separated into two single-peak curves.

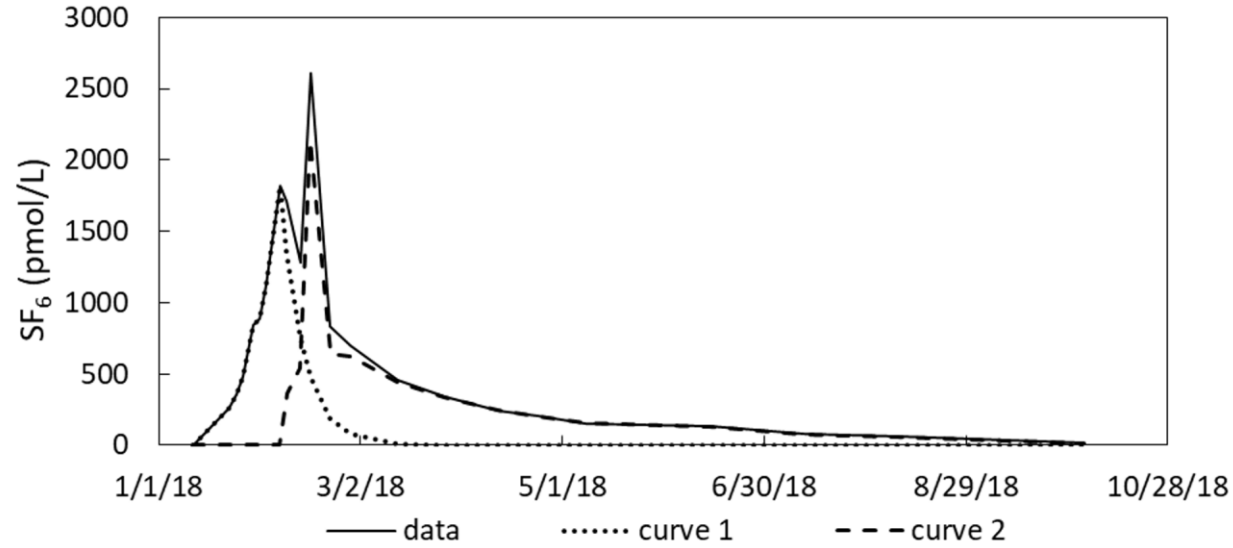

Figure S2.2: SF_6 breakthrough curve at MW-5 separated into two single-peak curves.